J. Fluid Mech. (1983), *vol.* 131, *pp.* 195–218
Printed in Great Britain

On inertial flow over topography. Part 1. Semigeostrophic adjustment to an obstacle

By L. J. PRATT†
Woods Hole Oceanographic Institution, Woods Hole, Massachusetts 02543

(Received 30 August 1982)

The nonlinear time-dependent adjustment of a homogeneous rotating-channel flow to the sudden obtrusion of an obstacle is studied. Solutions are obtained using a Lax–Wendroff numerical scheme which allows rotating breaking bores and jumps to form and be maintained. The flow upstream of the obstacle is found to be completely blocked, partially blocked (and hydraulically controlled), or unobstructed depending upon the height of the obstacle. Partial blockage is accomplished through the excitation of a combination of nonlinear Kelvin waves, some of which steepen into interfacial shocks. Riemann invariants for the Kelvin waves are found, and jump conditions on mass, momentum and potential vorticity for the shocks are discussed. The shocks are surrounded by dispersive regions of Rossby deformation scale, and the potential vorticity of passing fluid is altered at a rate proportional to the differential rate of energy dissipation along the line of breakage. For the special case of initially uniform potential vorticity the asymptotic state is found as a function of the initial conditions.

1. Introduction

A significant body of literature has been developed on the subject of large-scale geophysical flow over topography.‡ Most of this work has been done within the framework of quasigeostrophic theory, which assumes the Rossby number to be small. However, it is known that moderate to large Rossby numbers can be achieved where the constricting effect of the topography is large. A meteorological example is the severe downslope wind that is observed in the eastern Rocky Mountains (Klemp & Lilly 1975). Oceanic strait and sill flow such as occurs in the Denmark Strait (Worthington 1969) and coastal currents such as the Agulhas Current (Gill & Schumann 1979) can also be strongly inertial. The primary interest here will be in the oceanic case, where the current is strongly influenced by side walls as well as bottom relief. In addition to nonlinearity, the dynamical balance of such currents is often complicated by strong time dependence arising from hydrodynamic instabilities or external forcing, as exemplified in the current-meter records of Worthington (1969).

Previous investigations (e.g. Whitehead, Leetmaa & Knox 1974; Gill 1977; Shen 1981) of inertial strait and sill flow have concentrated on the behaviour of steady uniform-potential-vorticity flow in slowly varying channels. Special attention has been given to the 'hydraulics' of such flows, and, in particular, the conditions under

† Present address: Graduate School of Oceanography, University of Rhode Island, Kingston, RI 02881.

‡ A series of review papers appears in the World Meteorological Organization's *Orographic Effects in Planetary Flows*, *GARP Publ. Ser.* no. 23. World Met. Orgn.

which an obstacle or side contraction can control the upstream state (in the same way that a dam controls the level of a reservoir). However, the complication of time dependence has received little attention in rotating hydraulics (and hydraulics in general). This is odd, since time dependence is implicit in the physical notion behind the word 'control'. As Stern (1974) writes, a controlled state results if 'The free discharge of a fluid thru an open channel cannot remain unaltered when the width of the channel is reduced in the downstream direction, or when the height of the channel floor is raised.' An obstacle or contraction thus exercises control through time-dependent means. This idea can be seen in connection with non-rotating flow through the laboratory experiments of Long (1954, 1970), who towed an obstacle through a tank of (otherwise stagnant) fluid, and in the numerical experiments of Houghton & Kasahara (1967), who considered the sudden obtrusion of an obstacle into a uniform flow. In both cases obstacles of greater than a certain critical height induced a permanent response in the fluid which was eventually felt at great distances from the obstacle. This 'upstream influence' was set up by a combination of bores and rarefaction waves, which were generated near the obstacle during the initial adjustment. The asymptotic state (as time $\rightarrow \infty$) consisted of a new steady state whose flow rate was decreased from its initial value, and which occasionally contained a hydraulic jump in the lee of the obstacle.

The adjustment problem described above provides a useful way of understanding how steady solutions are established, how an obstacle exercises control over a flow, and how the flow might respond to other types of time-dependent forcing. The results indicate that free-surface shocks (bores and hydraulic jumps) and rarefaction waves play a crucial role in the adjustment of a controlled flow and in the asymptotic state itself. We will now investigate numerically the time-dependent adjustment of an inertial rotating-channel flow to the sudden obtrusion of an obstacle.

Part 1 of this series of papers deals solely with flows in slowly varying channels. This assumption leads to a semigeostrophic state in which the cross-stream momentum balance is geostrophic, while that along the stream is ageostrophic. The effects of wave dispersion tend to be suppressed in such a system, and the dynamics of adjustment appear to be similar to those of more-classical one-dimensional flows in which non-dispersive waves determine the outcome. It will be seen, for example, that Kelvin waves play the same role in the adjustment of a uniform-potential-vorticity flow that long gravity waves do in the experiments of Long (1954, 1970) and Houghton & Kasahara (1968). In Part 2, we will consider the influence of dispersive (Poincaré) waves, which arise when the assumption of slow variations is relaxed.

The format of Part 1 is as follows. In §§2 and 3 we derive the semigeostrophic equations and discuss some properties of nonlinear semigeostrophic waves for the special case in which the potential vorticity is uniform. In §4 we present numerical solutions to the adjustment problem and discuss the dependence of the asymptotic state on the initial conditions. Sections 5 and 6 contain analysis of the interfacial shocks that arise in the numerical solutions, including the derivation of an approximate relation for connecting the upstream and downstream states across a shock and discussion of the ability of the shock to alter potential vorticity. Finally, §7 contains a predictive theory for total flow blockage by the obstacle – a process which is beyond the capabilities of the numerical model.

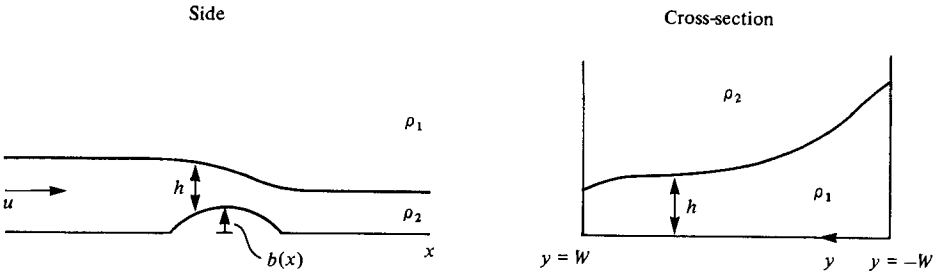

FIGURE 1. Definition sketch showing side and cross-sectional views of rotating channel.

2. Basic equations and the semigeostrophic approximation

The geometry to be considered (see figure 1) is that of a horizontal channel aligned in the x-direction and rotating with constant angular speed $\frac{1}{2}f$ about the vertical (z-axis). The channel contains vertical walls at $y = \pm W$ and bottom elevation $b(x)$ which varies on a horizontal scale L. A single inviscid layer of density ρ_2 flows beneath a deep inactive upper layer of density ρ_1 and extends entirely across the channel (no separation of the lower layer occurs). If D is a scale for $h(x, y, t)$, the thickness of the lower layer, then the hydrostatic approximation will be valid provided that $D/L \ll 1$. Under these conditions, the lower layer is described by the shallow-water equations (Pedlosky 1979). Using the dimensionless variables

$$x' = \frac{x}{L}, \quad y' = \frac{y}{W}, \quad t' = \frac{t(g'D)^{\frac{1}{2}}}{L},$$

$$u' = \frac{u}{(gD)^{\frac{1}{2}}}, \quad v' = \frac{vL}{(g'D)^{\frac{1}{2}}W}, \quad h' = \frac{h}{D}, \quad b' = \frac{b}{D},$$

and dropping primes, the following dimensionless shallow-water equations result:

$$u_t + uu_x + vu_y - Fv = -h_x - b_x, \tag{2.1}$$

$$\delta^2(v_t + uv_x + vv_y) + Fu = -h_y, \tag{2.2}$$

$$h_t + (uh)_x + (vh)_y = 0, \tag{2.3}$$

where

$$\delta = \frac{W}{L} \quad \text{(horizontal aspect ratio)},$$

$$F = \frac{Wf}{(g'D)^{\frac{1}{2}}} \quad \text{(width scale/Rossby radius of deformation)}$$

Note that the parameter F can be rewritten as

$$F = \frac{Wf}{(g'D)^{\frac{1}{2}}} = \frac{Wf}{U} = R_0^{-1},$$

where R_0 is a Rossby number. The parameter range $\delta \ll 1, R_0 \gg 1$ ($F \ll 1$) applies to classical hydraulics and categorizes the work of Long (1954, 1970) and Houghton & Kasahara (1968). Part 2 of this series will deal with the parameter setting $\delta = 1$ and $F = R_0 = 1$. Here we will be concerned with the 'semigeostrophic' limit in which the

flow is inertial ($R_0 = 1$) but varies slowly in the x-direction ($\delta \ll 1$). In this case (2.1)–(2.3) become

$$u_t + uu_x + vu_y - v = -h_x - \frac{db}{dx}, \tag{2.4}$$

$$u = -h_y + O(\delta^2), \tag{2.5}$$

$$h_t + (uh)_x + (vh)_y = 0, \tag{2.6}$$

From these follows the conservation law for potential vorticity

$$\left(\frac{\partial}{\partial t} + u\frac{\partial}{\partial x} + v\frac{\partial}{\partial y}\right)\phi = 0, \tag{2.7}$$

where

$$\phi = \frac{1 - u_y}{h} + O(\delta^2). \tag{2.8}$$

3. Time-dependent theory and steady solutions for ϕ = constant

Equation (2.5) implies that the lateral acceleration of fluid particles is unimportant in the cross-channel momentum balance. This dynamical restriction is reminiscent of the hydrostatic balance in which the vertical acceleration of fluid particles is neglected. Before proceeding to numerical solutions we pause to illuminate the consequences of (2.5) by discussing an analytic theory for the special case in which ϕ = constant. The development begins along the lines of Gill (1977), who found steady solutions containing uniform ϕ. We start by combining (2.5) and (2.8) to form a single equation for h:

$$h_{yy} - \phi h = -1.$$

For $\phi > 0$, the solution can be written as

$$h = \phi^{-1} + A(x,t)\frac{\sinh(\phi^{\frac{1}{2}}y)}{\sinh(\phi^{\frac{1}{2}}w)} + B(x,t)\frac{\cosh(\phi^{\frac{1}{2}}y)}{\cosh(\phi^{\frac{1}{2}}w)}, \tag{3.1}$$

where w is the channel half-width. It follows from (2.5) that

$$u = -\phi^{\frac{1}{2}}\left[A(x,t)\frac{\cosh(\phi^{\frac{1}{2}}y)}{\sinh(\phi^{\frac{1}{2}}w)} + B(x,t)\frac{\sinh(\phi^{\frac{1}{2}}y)}{\cosh(\phi^{\frac{1}{2}}w)}\right]. \tag{3.2}$$

For $\phi^{\frac{1}{2}} \gg 1$ the flow thus becomes confined to sidewall boundary layers.

Following Gill we now introduce the following dependent variables:

$$\bar{h} = \tfrac{1}{2}[h(x,w,t) + h(x,-w,t)] = \phi^{-1} + B(x,t), \tag{3.3}$$

$$\Delta h = \tfrac{1}{2}[h(x,w,t) - h(x,-w,t)] = A(x,t), \tag{3.4}$$

$$\bar{u} = \tfrac{1}{2}[u(x,w,t) + u(x,-w,t)] = -\phi^{\frac{1}{2}}T^{-1}A(x,t), \tag{3.5}$$

$$\Delta u = \tfrac{1}{2}[u(x,w,t) - u(x,-w,t)] = -\phi^{\frac{1}{2}}TB(x,t), \tag{3.6}$$

where $T = \tanh(w\phi^{\frac{1}{2}})$.

From these it follows that

$$\bar{u} = -\phi^{\frac{1}{2}}T^{-1}\Delta h, \tag{3.7}$$

$$\Delta u = \phi^{\frac{1}{2}}T(\phi^{-1} - \bar{h}). \tag{3.8}$$

To find the x- and t-dependence of the solution, we evaluate (2.4) on either sidewall and apply the boundary condition

$$v_{\pm} = 0 \quad (y = \pm w). \tag{3.9}$$

Taking the sum of the results and applying (3.3)–(3.6) yields

$$2\bar{u}_t + (\bar{u}^2 + \Delta u^2 + 2\bar{h})_x = -2\frac{\mathrm{d}b}{\mathrm{d}x}, \tag{3.10}$$

while the difference gives

$$\Delta u_t + (\bar{u}\,\Delta u + \Delta h)_x = 0. \tag{3.11}$$

Equations (3.7) and (3.8) can now be used to eliminate Δu and $\bar{u}$ in favour of Δh and $\bar{h}$. Thus (3.10) and (3.11) become

$$\Delta h_t - (\phi^{\frac{1}{2}}T^{-1}\Delta h)\,\Delta h_x + [\phi^{\frac{1}{2}}T^3(\phi^{-1} - \bar{h}) - T\phi^{-\frac{1}{2}}]\,\bar{h}_x = T\phi^{-\frac{1}{2}}\frac{\mathrm{d}b}{\mathrm{d}x}, \tag{3.12}$$

$$\bar{h}_t - (\phi^{\frac{1}{2}}T^{-1}\bar{h})\,\Delta h_x - (\phi^{\frac{1}{2}}T^{-1}\Delta h)\,\bar{h}_x = 0. \tag{3.13}$$

We now have two equations for $\bar{h}$ (the average of the side depths) and Δh (the difference in side depth, and therefore a measure of velocity). Steady solutions can be found by noting that the steady versions of (3.12) and (3.13) are exact differentials. Integration with respect to x yields a Bernoulli equation

$$T^{-2}\phi\,\Delta h^2 + \phi T^2(\phi^{-1} - \bar{h})^2 + 2\bar{h} = -2b(x) + 2\bar{B}, \tag{3.14}$$

and a mass-conservation statement

$$\Delta h\,\bar{h} = -Q, \tag{3.15}$$

where $\bar{B}$ is the average of the Bernoulli constant $\frac{1}{2}u^2 + b + h$ on either wall and Q is the rate of flow. Equations (3.14) and (3.15) can be combined to form the following quartic equation for $\bar{h}$:

$$\phi T^2(\phi^{-1} - \bar{h})^2\,\bar{h}^2 + 2\bar{h}^3 + 2(b(x) - \bar{B})\,\bar{h}^2 + T^{-2}\phi Q^2 = 0. \tag{3.16}$$

Gill (1977) discusses the properties of the solutions to (3.16) in detail using a slightly different set of parameters.† Here we simply sketch a family of solutions obtained by holding Q constant and considering various values of $\bar{B}$. The bottom topography consists of an isolated obstacle, and the solutions are drawn (figure 2) in terms of the interface elevation along the wall at $y = w$ (as computed from $h(w) = \bar{h} + \Delta h$). It can be seen that two distinct solutions exist for each large value of $\bar{B}$ and that each maintains the same depth on either side of the obstacle. As B is reduced, however, a critical value ($\bar{B} = 4.29$) is reached at which the two curves coalesce over the sill of the obstacle. Here it is not obvious which branch is correct. After moving along the interface curve from ① to ③, for example, it is not clear whether one should proceed to ④ or ⑤. Based on physical intuition we would likely choose ⑤, since this branch resembles the commonly observed configuration of fluid flowing over a dam or weir.

If $\bar{B}$ is further reduced the solutions no longer extend across the entire obstacle. The energy of the flow has been reduced to the point where the fluid cannot surmount the sill. The solution for $B = 4.29$ contains the minimum energy necessary, and is therefore 'controlled' in the sense that a small increase in the sill height would necessitate a time-dependent change in the upstream conditions for flow to continue. Such upstream influence would not be necessary for the other continuous solutions since they contain energy in excess of the required amount.

Some of the time-dependent properties of (3.12) and (3.13) are revealed through

† In place of $\bar{B}$, Gill uses a parameter that measures the partitioning of the flow into the sidewall boundary layers.

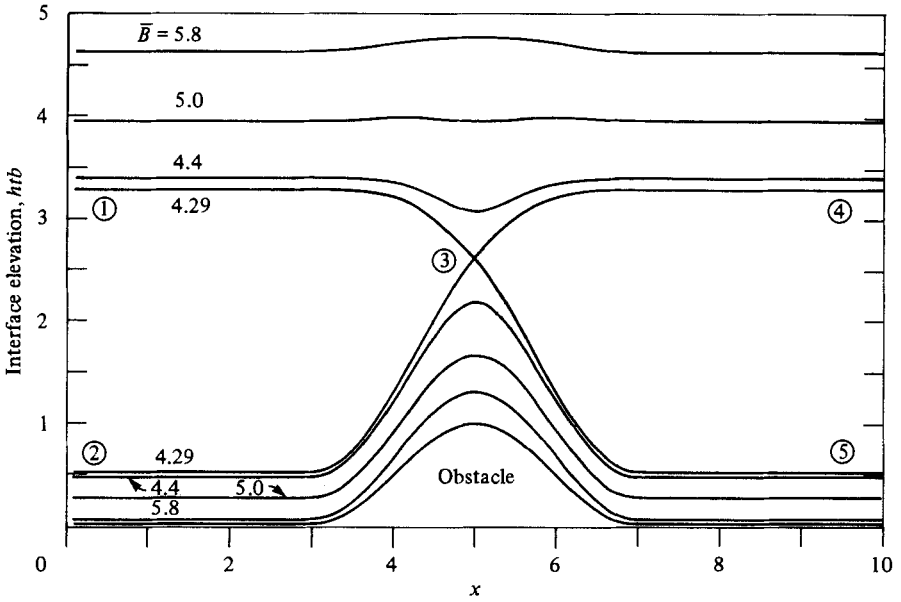

FIGURE 2. Steady solutions for flow over obstacle showing interface elevations along the side wall. The family of interface profiles are obtained by fixing $Q = \phi = 1.0$ and varying $\bar{B}$. The flow at the coalescence point (labelled ③) is critical with respect to the Kelvin wave speed.

reformulation in terms of characteristics. Equations (3.12) and (3.13) form a quasilinear system which can be written in the form

$$\frac{\partial u_i}{\partial t} + a_{ij}\frac{\partial u_j}{\partial x} = b_i, \tag{3.17}$$

where

$$\left.\begin{aligned} u_i &= (\Delta h \quad \bar{h}), \\ a_{ij} &= \phi^{\frac{1}{2}}T^{-1}\begin{pmatrix} \Delta h & T^4(\phi^{-1}-\bar{h}) - T^2\phi^{-\frac{1}{2}} \\ \bar{h} & -\Delta h \end{pmatrix}, \\ b_i &= \begin{pmatrix} T\phi^{-\frac{1}{2}}\dfrac{\mathrm{d}b}{\mathrm{d}x} & 0 \end{pmatrix}. \end{aligned}\right\} \tag{3.18}$$

The characteristic speeds are given (Whitham 1974) by the eigenvalues of a_{ij}, namely

$$\begin{aligned} \lambda_\pm &= -\phi^{\frac{1}{2}}T^{-1}\Delta h \pm \bar{h}^{\frac{1}{2}}[1-T^2(1-\phi\bar{h})]^{\frac{1}{2}} \\ &= \bar{u} \pm \bar{h}^{\frac{1}{2}}[1-T^2(1-\phi\bar{h})]^{\frac{1}{2}}, \end{aligned} \tag{3.19}$$

and can be interpreted as the x-speeds of wave fronts propagating into an undisturbed region characterized by Δh and $\bar{h}$. An alternative interpretation is that $\lambda_\pm$ represent the phase speeds of infinitesimal waves propagating on a current characterized by uniform values of $\bar{u}$ and $\bar{h}$. For narrow channels ($T^2 \to 0$) $\lambda_\pm$ reduce to $u \pm h^{\frac{1}{2}}$, the speeds of long gravity waves. As it stands we may interpret $\lambda_\pm$ as the speeds of Kelvin waves being advected at rate $\bar{u}$ and propagating at relative rates $\pm\bar{h}^{\frac{1}{2}}[1-T^2(1-\phi\bar{h})]^{\frac{1}{2}}$. Since $T^2 \leqslant 1, \lambda_\pm$ will always be real, and consequently (3.12) and (3.13) will be hyperbolic.

Returning to figure 2, we now inquire into the properties of the steady solutions with respect to wave propagation. At the sill of the obstacle, the minimum value of

$\bar{B}$ occurs where the solutions coalesce (labelled ③). Taking $\partial\bar{B}/\partial\bar{h} = 0$ (with Q and b fixed) in (3.16) leads to the result that the flow is *critical*, $\lambda_- = 0$, at the coalescence point. Using Δh_c and $\bar{h}_c$ to denote the values of Δh and $\bar{h}$ at the critical point,

$$\phi^{\frac{1}{2}}T^{-1}\Delta h_c = -\bar{h}_c^{\frac{1}{2}}[1-T^2(1-\phi\bar{h}_c)]^{\frac{1}{2}}, \tag{3.20}$$

in view of (3.19). It is easily verified that the flow is subcritical ($\lambda_- < 0$) for $\bar{h} > \bar{h}_c$ and supercritical ($\lambda_- > 0$) for $\bar{h} < \bar{h}_c$.

The characteristic forms of (3.12) and (3.13) provide interpretative aids in understanding the nonlinear evolution of the Kelvin waves. Following Whitham (1974) the characteristic forms, obtained through multiplication of (3.17) by eigenvectors $l_{i\pm}$ satisfying $l_{i\pm}(a_{ij}-\lambda_\pm) = 0$, are

$$-\phi^{\frac{1}{2}}T^{-1}\bar{h}\frac{\mathrm{D}_\pm}{\mathrm{D}t}\Delta h + (\phi^{\frac{1}{2}}T^{-1}\Delta h + \lambda_\pm)\frac{\mathrm{D}_\pm}{\mathrm{D}t}\bar{h} = -\bar{h}\frac{\mathrm{d}b}{\mathrm{d}x}, \tag{3.21}$$

where

$$\frac{\mathrm{D}_\pm}{\mathrm{D}t} = \frac{\partial}{\partial t} + \lambda_\pm\frac{\partial}{\partial x}$$

is a derivative taken along characteristic curves with slope $\lambda_\pm$. A simplified version of (3.21) can be obtained through division by $\bar{h}$ and integration by parts of the second term on the left. The result is

$$\frac{\mathrm{D}_\pm}{\mathrm{D}t}R_\pm = -\frac{\mathrm{d}b}{\mathrm{d}x}, \tag{3.22}$$

with the *Riemann variables* $R_\pm$ defined by

$$R_\pm = \bar{u} \pm \{(\bar{h}(1-T^2)+T^2\phi\bar{h}^2)^{\frac{1}{2}} + \tfrac{1}{2}T^{-1}\phi^{-\frac{1}{2}}(1-T^2) \times \ln[2T\phi^{\frac{1}{2}}(\bar{h}(1-T^2)+T^2\phi\bar{h}^2)^{\frac{1}{2}} + 2T^2\phi\bar{h} + (1-T^2)]\}. \tag{3.23}$$

Using a Taylor expansion for the logarithm it is easy to verify that $R_\pm$ approaches the non-rotating limit $\bar{u} \pm 2\bar{h}^{\frac{1}{2}}$ as $T \to 0$. As is the case in this limit, the Riemann variable is conserved following characteristics, provided that the bottom is flat ($\mathrm{d}b/\mathrm{d}x = 0$). It is further evident from (3.19) and (3.23) that $\lambda_\pm$ and $R_\pm$ behave monotonically with respect to $\bar{h}$ (e.g. λ_+ and R_+ increases with increasing $\bar{h}$, for $\bar{h} > 0$). This property can be used to show that the nonlinear steepening and spreading properties of the Kelvin waves depend upon $\bar{u}$ and $\bar{h}$ in a way similar to that of long gravity waves on u and h. The argument is an extension of the standard argument for long gravity waves as described in Stoker (1957). Picture, for example, a Kelvin wave front entering an undisturbed region of the channel where the flow is characterized by uniform values of $\bar{h}$ and Δh. The front can be considered a continuum of wavelets, each with speed λ_+ (say) and each carrying a non-changing value of R_+. As the front propagates through the undisturbed region it must maintain a *uniform* value of R_-, as required by (3.22). Thus, if the wave tends to increase $\bar{h}$ over its undisturbed value it must also increase $\bar{u}$ in order to conserve R_-. The wave speed λ_+ must also increase, in view of (3.19), implying a steepening of the wave front. In general, one finds that waves of elevation (measured in terms of $\bar{h}$) tend to steepen and break while those of depression tend to spread in the manner of a rarefaction wave.

The adjustment of a uniform-potential-vorticity flow will be accomplished through generation of the waves described above. In the small-amplitude limit, these waves can be identified as Kelvin waves modified by the non-uniform flow upon which they

propagate. Large-amplitude waves will tend to steepen or spread nonlinearly in the manner of long gravity waves.

4. Numerical solutions to the adjustment problem

We now study the establishment of steady solutions through an adjustment problem similar in design to the experiments of Long (1954) and Houghton & Kasahara (1968). The initial state consists of a subcritical ($\lambda_- < 0$), geostrophically balanced, steady flow with velocities $u = u_0(y)$, $v = 0$, and depth $h = h_0(y)$ over a flat bottom. At $t = 0$ an obstacle appears in the channel and the resulting motion is computed numerically. The numerical scheme consists of a two-step Lax–Wendroff finite-difference method which integrates the full set of two-dimensional shallow-water equations (2.1)–(2.3). The obstacle has a small horizontal aspect ratio ($\delta \approx \frac{1}{6}$), so that the flow is approximately semigeostrophic. The Lax–Wendroff scheme allows interfacial shocks to form and be maintained in the interior of the rectangular mesh, ensuring that mass and momentum flux is conserved across the shocks. The numerical scheme is presented in more detail in appendix A.

In order to make comparisons with the theory discussed in §3, we first consider the case in which the initial potential vorticity is uniform and positive:

$$\frac{1-u_{0y}}{h_0} = \phi = \text{constant} > 0.$$

In this case the adjustment that occurs and the asymptotic state that results are found to depend crucially upon the height of the obstacle b_0 in relation to a critical height b_c. This critical height is the maximum obstacle height for which a *steady* flow with parameters $Q = Q_0$ and $B = B_0$ is able to exist. In other words, given the initial parameters B_0 and Q_0 it is possible to find a family of steady solutions having flow rate Q_0 and 'energy' B_0 for flow over obstacles of heights $b \leqslant b_c$. When $b = b_c$ the flow contains the minimal amount of energy needed to exist, and therefore becomes critical at the obstacle's sill, as indicated in figure 2. Therefore

$$b_c = \bar{B}_0 - \tfrac{1}{2}T^{-2}\phi\,\Delta\bar{h}_c^2 - \tfrac{1}{2}\phi T^2(\phi^{-1}-\bar{h}_c)^2 - \bar{h}_c, \tag{4.1}$$

in view of (3.14).

An expression for b_c in terms of Q_0 and $\bar{B}_0$ can be obtained through the use of (3.15) applied at the sill and the critical condition (3.20):

$$\bar{h}_c^4 + \phi^{-1}(T^{-2}-1)\,\bar{h}_c^3 - T^{-4}Q_0^2 = 0, \tag{4.2}$$

while (3.20) and (4.1) combine to give

$$b_c = \bar{B}_0 - \tfrac{1}{2}\phi T^2(\phi^{-1}-\bar{h}_c)\,(\phi^{-1}-2\bar{h}_c) - \tfrac{3}{2}\bar{h}_c. \tag{4.3}$$

Together (4.2) and (4.3) give b_c in terms of Q_0 and B_0 with $\bar{h}_c$ an intermediate variable. A plot of b_c as a function of B_0 with $Q_0 = 1$ appears in figure 9. Unfortunately, there appears to be no simple way of displaying this information in terms of a Froude number, as is done in connection with non-rotating flows.

The adjustment that occurs when $b_0 < b_c$ is shown in figure 3. The obstacle is drawn in the lower frame and the upper three frames show perspective views of the interface after various time steps. After 20 time steps (one rotation period), the interface has begun to bulge over the newly formed obstacle. After 60 steps, this bulge has broken into two isolated Kelvin waves – one that moves upstream along the near wall and the other downstream along the far wall. At 100 time steps, these waves have moved

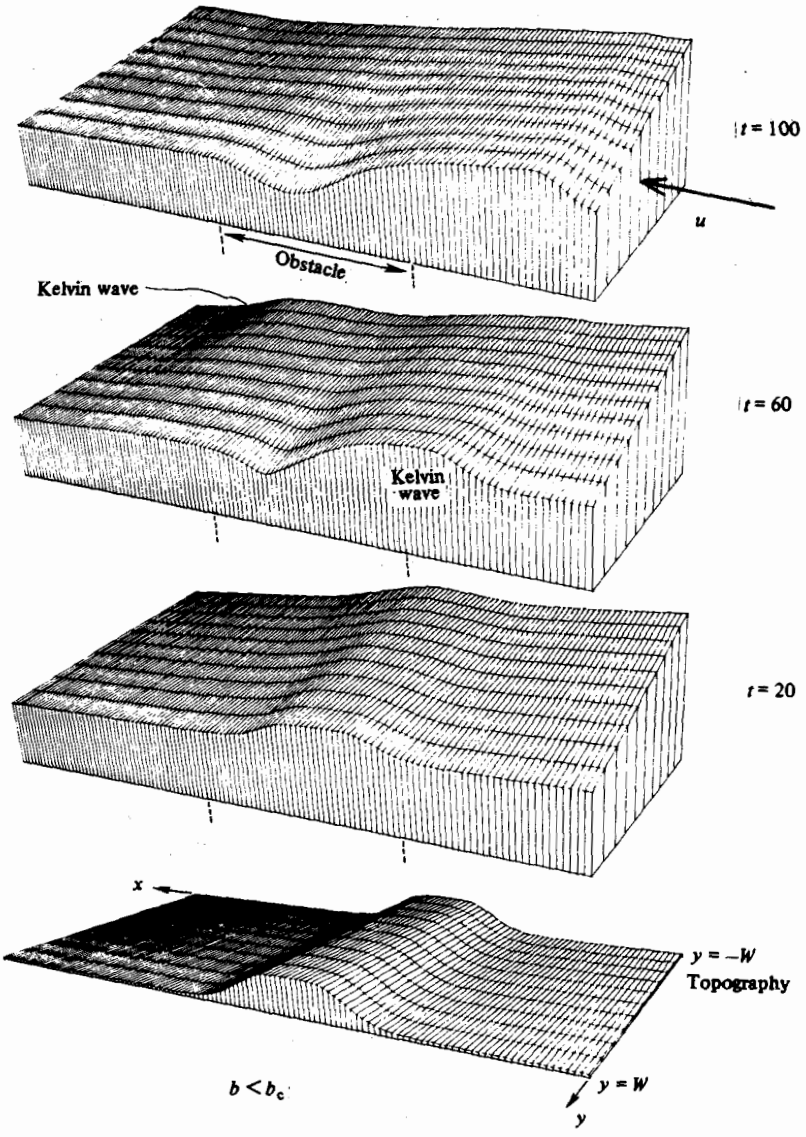

FIGURE 3. Adjustment of an initially subcritical flow for the case $b_0 < b_c$. The initial potential vorticity is uniform. The obtruded obstacle is shown in the lower frame and the evolution of the interface in the upper three frames. The parameter settings are $\phi_0 = 1.4$, $T = 0.8$, $Q_0 = 0.5$, $\bar{B}_0 = 1.5$, $b_c = 0.2$, $b_0 = 0.15$.

away from the obstacle, leaving behind a steady flow which resembles one of the subcritical curves of figure 2. The Kelvin waves only temporarily disturb the flow away from the obstacle: after the waves pass the flow fields return to their initial values. We therefore say that the obstacle exerts no *upstream influence* since no permanent response is induced in the flow away from the obstacle and the asymptotic state can be computed directly from (3.16) using the initial values $\bar{B}_0$ and Q_0.

If $b_0 \geqslant b_c$ the adjustment is quite different, as shown in figure 4. Instead of isolated Kelvin waves, the bulge now develops into bores which are trapped against the sidewalls in the manner of the Kelvin waves. After 80 time steps, these bores have

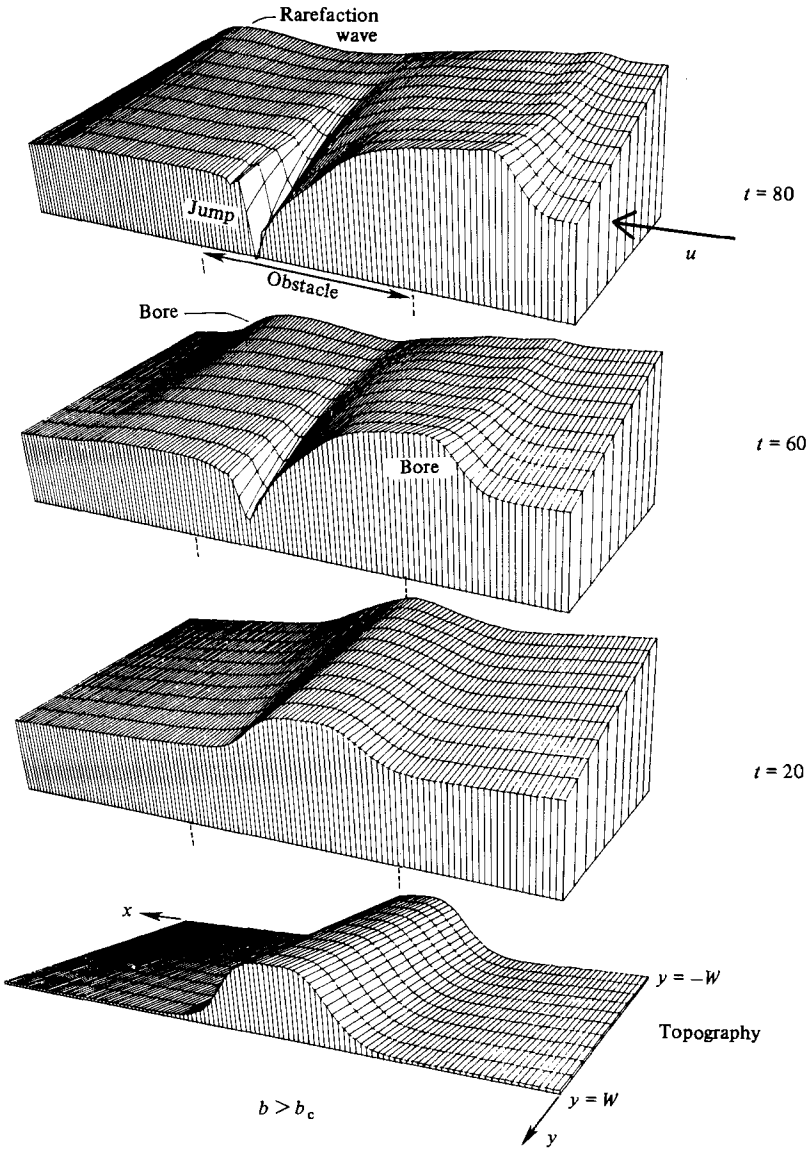

FIGURE 4. Adjustment for $b_0 > b_c$ showing establishment of hydraulically controlled flow. The initial conditions are identical with those of figure 3 except for the obstacle height $b_0 = 0.25$.

moved completely away from the obstacle and have nearly steepened to the point of breakage. The downstream-moving bore is trailed by a rarefaction wave which is beginning to spread (also see figure 5). The bores leave behind a steady flow which resembles solution curve ①–⑤ of figure 2 and contains a hydraulic jump in the lee of the sill. This steady flow contains a flow rate which is decreased from the initial value and can be termed *partially blocked*. The critical condition (4.3) is satisfied (within a tiny error) at the sill. Here the obstacle clearly has established upstream influence through generation of the upstream bore. Further increases in the height of the obstacle lead to a repetition of this chain of events and the establishment of a new critical state over the obstacle.

The determination of the asymptotic state when $b_0 \geqslant b_c$ is more subtle. In the non-rotating analogue of this problem, Houghton & Kasahara (1968) connected the initial state far from the obstacle to the flow over the obstacle using the Rankine–Hugoniot jump conditions and the fact that a critical condition exists over the obstacle. The same procedure should be possible here provided that the appropriate jump conditions are known. This problem is taken up in §§5 and 6.

Inspection of the hydraulic jump in the top frame of figure 4 reveals the presence of short parasitic waves in the lee. These waves are numerical oscillations which are commonly found in shock computations using Lax–Wendroff schemes. A small artificial viscosity was found necessary to keep these numerical instabilities under control (appendix A). Despite this, it was possible to make stable computations over only 400 or 500 time steps, after which time the numerical oscillations grew unacceptably large.

The results above were obtained using subcritical initial states. Some supercritical cases were also computed, with the results considerably noisier. However the adjustment proved to be similar to that shown in figure 4 with the asymptotic state again resembling solution ①–⑤ of figure 2. In no case was the branch ②–④ realized.

A series of numerical solutions were also obtained for the following initial state:

$$\left.\begin{aligned} u_0 &= a = \text{constant}, \\ h_0 &= 1 + ay \quad (-0.5 \leqslant y \leqslant 0.5), \end{aligned}\right\} \tag{4.4}$$

leading to the non-uniform potential-vorticity distribution

$$\phi_0 = (1+ay)^{-1}.$$

Because of the lack of an analytic theory for flows with non-constant ϕ, the dependence of the asymptotic state on the obstacle height is more difficult to formulate. However, the intuition gained regarding the energy argument made for uniform-ϕ flows suggests that some critical obstacle height b_c should exist which determines the nature of the adjustment. The numerical experiments carried out using initial state (4.4) supported this idea. For b_0 less than an (unknown) critical height b_c the adjustment was similar to that of figure 3, with no upstream influence imparted by the obstacle. An actual solution for $b_0 > b_c$ and $a = 0.7$ is shown in figure 5 using longitudinal sections of the flow to display the results. The bores, rarefaction wave and hydraulic jump are again present and are responsible for the apparent establishment of a hydraulically controlled state. It is not known, however, whether this similarity will continue to exist on longer timescales.

5. Shock connection

The interfacial shocks that arise in the partially blocked solutions play crucial roles in both the adjustment process and the asymptotic state. The rotating hydraulic jump pictured in figure 4 might serve as a possible explanation for the mixing that is often observed downstream of oceanic sills. We now make a closer examination of these interfacial shocks and try to determine how upstream and downstream states are connected. The following development neglects the entrainment of upper-layer fluid that might occur in a laboratory experiment but which is disallowed by the numerical scheme. For this reason, the theory presented below might more accurately be described as a *free-surface* shock theory.

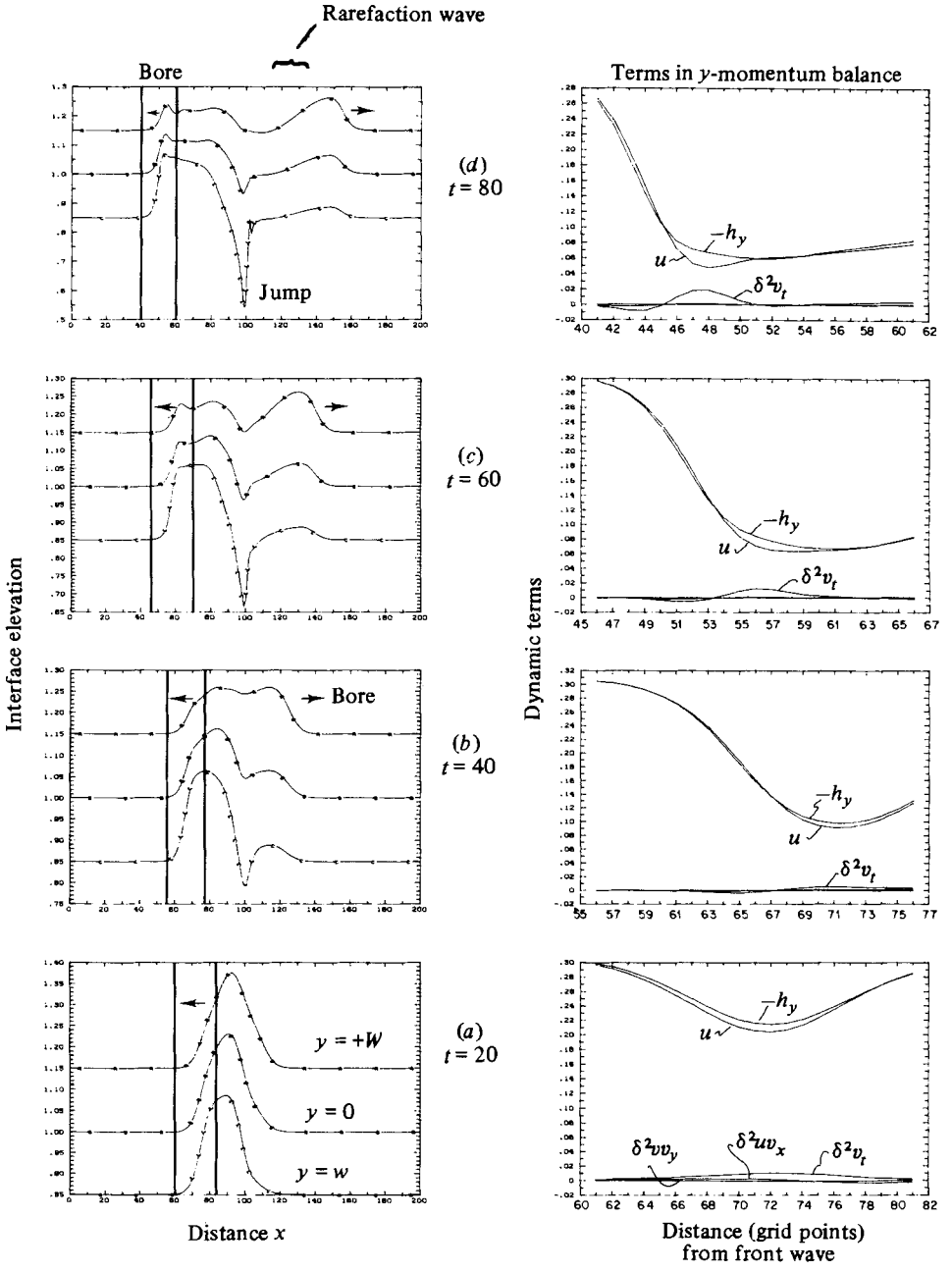

FIGURE 5. Adjustment of flow containing non-uniform potential vorticity to an apparent hydraulically controlled state. The left-hand figures show the evolution of the interface along longitudinal sections taken near the wall at $y = -w$ (labelled A), at mid-channel (labelled B), and along the wall at $y = w$ (labelled C). The right-hand figures show the y-momentum balance at mid-channel across the upstream-moving wave. As this wave steepens, the dispersive term $\delta^2 v_t$ becomes increasingly significant. The initial potential vorticity varies linearly from a value of 1.5 at $y = +w$ to 0.75 at $y = -w$, $b_0 = 0.25$, $Q_0 = 0.7$ and $\bar{B}_0 = 0.15$.

Let us first relax the narrow-channel approximation and consider a shock which exists in a channel flow of arbitrary width. Although the interior of the shock is a complicated region in which the shallow-water approximation breaks down, no sources of mass or momentum flux are present and we may connect the upstream and downstream states by integrating the conservation laws for mass and momentum flux across the discontinuity. The conservation laws for momentum flux are obtained by multiplication of (2.1)–(2.3) (with $\delta = R_0 = 1$) by h, integration by parts, and application of (2.3). The results are

$$(uh)_t + (u^2h + \tfrac{1}{2}h^2)_x + (uvh)_y = -h\frac{\mathrm{d}b}{\mathrm{d}x} + hv, \tag{5.1}$$

$$(vh)_t + (uvh)_x + (v^2h + \tfrac{1}{2}h^2)_y = -uh. \tag{5.2}$$

The continuity equation

$$h_t + (uh)_x + (vh)_y = 0 \tag{5.3}$$

is already in conservation-law form.

Without any loss in generality, we can rotate the (x, y)-coordinates into (n, s)-coordinates such that s is measured tangent to the shock and n normal to the shock at some point P. Upon integration across the shock and shrinkage of the interval of integration to zero, only contributions from the n- and t-derivatives will remain finite. For example, integration of the continuity equation (5.3) from $A < \eta(P)$ to $B > \eta(P)$ gives

$$\int_B^A \{h_t + (u^{(n)}h)_n + (u^{(s)}h)_s\}\,\mathrm{d}n = \int_A^\eta h_t\,\mathrm{d}n + \int_\eta^B h_t\,\mathrm{d}n + u_B^{(n)}h_B - u_A^{(n)}h_A + \int_A^B (u^{(s)}h)_s\,\mathrm{d}n,$$

where η is the n-position of the shock and $(u^{(n)}, u^{(s)})$ are the normal and tangential velocities. Applying Leibnitz's rule to the first two terms on the right-hand side of the above equation and letting $A \to \eta_-$, and $B \to \eta_+$, we find

$$(h_A - h_B)\frac{\mathrm{d}\eta}{\mathrm{d}t} + u_B^{(n)}h_B - u_A^{(n)}h_A = 0$$

or

$$c\left[h\right]_A^B - \left[u^{(n)}h\right]_A^B = 0 \tag{5.4}$$

where

$$\left[(\ )\right]_A^B = (\ )_A - (\ )_B$$

and $c = \mathrm{d}\eta/\mathrm{d}t$ is the velocity of the shock normal to itself. Similarly, integration of (5.1) and (5.2) yields

$$c\left[u^{(n)}h\right]_A^B - \left[u^{(n)2}h + \tfrac{1}{2}h^2\right]_A^B = 0, \tag{5.5}$$

$$c\left[u^{(s)}h\right]_A^B - \left[u^{(n)}u^{(s)}h\right]_A^B = 0. \tag{5.6}$$

Equations (5.4) and (5.5) are the familiar Rankine–Hugoniot conditions on mass and momentum flux that apply to one-dimensional shocks. The third relation can be simplified to

$$\left[u^{(s)}\right]_A^B = 0 \tag{5.7}$$

upon combination with (5.4). Therefore the tangential velocity is continuous, implying that the potential vorticity $(1 + \partial u^{(s)}/\partial n - \partial u^{(n)}/\partial s)/h$ of a fluid parcel crossing the shock must remain finite – though not necessarily conserved.

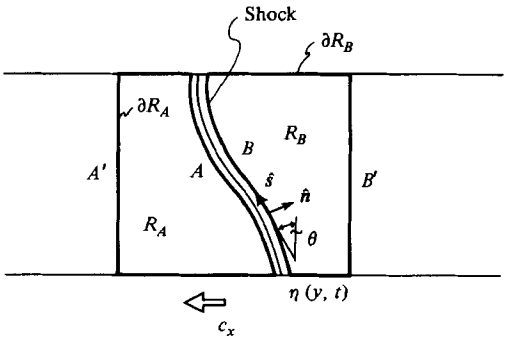

FIGURE 6. Plan view of channel showing shock and surrounding dispersive region. The dispersive influence is confined to R_A and R_B, and the entire pattern translates to the left at speed C_x.

If $u^{(s)} \neq 0$, then (5.4) and (5.7) further imply that the velocity vector must change direction upon passing the shock. This demands that the shock become perpendicular to any solid boundary at the point of that contact, otherwise the shock would induce a flow normal to the boundary. More generally, the shock must become aligned perpendicular to x as $v/u \to 0$.

In general, given $u_A^{(n)}$, $u_A^{(s)}$ and h_A one can compute the downstream fields $u_B^{(n)}$, $u_B^{(s)}$ and h_B using (5.4), (5.5) and (5.7), provided that c is known. The semigeostrophic case is apparently simpler since the ratio of (dimensional) v to u approaches zero and the entire shock should be described by a single velocity c. Under these conditions, it is tempting to describe the shock as a *weak* solution to the semigeostrophic equations (2.4)–(2.6). In such a description the flow would be semigeostrophic at all points not on the shock. However, equations (5.4), (5.5) and (5.7) make no allowance for geostrophy. Being proportional to velocity (and not its derivative) rotational terms must act over a finite distance and therefore do not appear in (5.4)–(5.7). Given a semigeostrophic upstream state, for example, there is no guarantee that the velocity u_B immediately downstream of the shock (as computed using (5.4), (5.5) and (5.7)) will be in geostrophic balance with h_B. We therefore submit that the shock is bordered by a region in which the terms $\delta^2(v_t + uv_x + vv_y)$ becomes as large as u and h_y and therefore in which lateral dispersion becomes important. The width of this dispersive region is $O(\delta)$ (the deformation radius) and its role is to adjust the shock to the semigeostrophic flow on either side.

Figure 5 shows the importance of lateral dispersion (as reflected by the y-momentum balance) as a front steepens into a bore. The information is taken from the upstream moving front shown in the left-hand side of the figure. Initially the flow is semigeostrophic (figure 5*a*) but the geostrophic balance weakens as the front steepens. This is due to the tendency of the front to counter the cross-channel interface tilt. Meanwhile, the term $\delta^2 v_t$ is becoming significant over an $O(\delta)$ interval about the front (figures 5*b*, *c*).

Is it possible to connect the flow upstream of the dispersive region to that downstream without resolving the complicated region in between? In general, the answer is no. However, it is possible to derive approximate formulas for special cases. One such case is typified by the shocks observed in the numerical experiments. Once formed, these shocks and their surrounding dispersive region were observed to translate with little change in form at a fixed speed c_x along the channel. For such shocks, one might be tempted to simply equate the net mass and momentum flux upstream and downstream of the translating region. Referring to figure 6, this

procedure would involve integrating the mass and momentum flux over sections A' and B' (which represent the outer extremities of the dispersive regions R_A and R_B) and equating the results, thereby neglecting any mass and momentum that is added to R_A and R_B. In terms of momentum, such an integration leads to

$$\left[\int_{-w}^{w} \{(u-c_x)\,uh+\tfrac{1}{2}h^2\}\,\mathrm{d}y\right]_{A'}^{B'} = -\iint_{R_A+R_B} h\left(\frac{\mathrm{d}b}{\mathrm{d}x}-v\right)\mathrm{d}\sigma, \tag{5.8}$$

as shown in appendix B. Momentum flux can thus be gained in R_A+R_B through bottom topography ($h\,\mathrm{d}b/\mathrm{d}x$) and rotation ($hv$). However, since the area of R_A+R_B is $O(\delta^2)$, the right-hand side of (5.8) is $O(\delta^2)$ while the left is $O(\delta)$. This allows us to write

$$\frac{1}{\delta}\left[\int_{-w}^{w} \{(u-c_x)\,uh+\tfrac{1}{2}h^2\}\,\mathrm{d}y\right]_{A'}^{B'} = O(\delta) \tag{5.9}$$

(i.e. an error $O(\delta)$ is incurred in equating the net momentum flux across the shock and dispersive region). The corresponding restriction on mass flux,

$$\left[\int_{-w}^{w} (u-c_x)\,h\,\mathrm{d}y\right]_{A'}^{B'} = 0, \tag{5.10}$$

can, of course, be made with no error.

An alternative statement of momentum-flux conservation which is accurate to the same order can be derived through integration along the side walls, rather than over R_1 and R_2. Taking advantage of the fact that $v = 0$ at the wall, we find

$$\left[(u_\pm-c_x)\,u_\pm h_\pm+\tfrac{1}{2}h_\pm^2\right]_{A'}^{B'} = O(\delta), \tag{5.11}$$

whereas $\pm$ denote the values at $\pm w$. The values of u_+ and h_+ at A' and B' can be related to u_- and h_- through (3.3)–(3.8). Equations (5.9) and (5.11) are accurate to $O(\delta)$ while semigeostrophy is accurate to $O(\delta^2)$.

Suppose $u_{A'}(y)$, $h_{A'}(y)$ (and thus $\phi_{A'}(y)$) and c_x are given. Are $u_{B'}(y)$ and $h_{B'}(y)$ then uniquely determined by (5.9) and (5.10)? Since the flow at B' is semigeostrophic, (3.22) and (3.25) can be combined to form a single equation for $h_{B'}$:

$$\frac{\partial^2}{\partial y^2}h_{B'}-\phi_{B'}h_{B'} = -1. \tag{5.12}$$

For suitably well-behaved $\phi_{B'}(y)$, solutions will exist and contain two arbitrary constants. Equations (5.9) provide two equations for their values, provided that (5.12) can be solved. However, the solution depends on the potential vorticity at B', which is yet unknown. If $\phi(y)$ does not change from A' to B' by more than an $O(\delta)$ amount, it is self-consistent to set $\phi_{A'}(y) = \phi_{B'}(y)$. However, the jump conditions (5.4)–(5.7) say nothing about continuity of ϕ at the shock, but only that it remains finite. Furthermore, the displacement of streamlines that occur across a moving jump can lead to a rearrangement of the distribution of ϕ across the channel. We next return to the equations of motion and the numerical model in an attempt to gain more insight into the behaviour of ϕ near a discontinuity.

6. The change in potential vorticity across a shock

Again consider a shock and dispersive region that translate along the channel (figure 6). The momentum equations (2.1)–(2.3) with $\delta = 1$ for the flow become in vector form

$$-c_x \frac{\partial \boldsymbol{u}}{\partial x} + (\boldsymbol{u}\cdot\nabla)\boldsymbol{u} - k\times\boldsymbol{u} + \nabla(h+b) = 0. \tag{6.1}$$

As before, we rotate the coordinates (x, y) into new coordinates (n, s) such that s is tangent to the shock at a point P. Thus

$$\frac{\partial}{\partial x} = \cos\theta \frac{\partial}{\partial n} - \sin\theta \frac{\partial}{\partial s}, \tag{6.2}$$

where θ is measured between the shock and the y-axis.

By definition, the change in potential vorticity across the shock can be expressed as

$$\underset{A}{[}\phi\underset{B}{]} = \left[\frac{1}{h}\right]_{A}^{B} - \left[\frac{\partial u^{(n)}/\partial s}{h}\right]_{A}^{B} + \left[\frac{\partial u^{(s)}/\partial n}{h}\right]_{A}^{B}, \tag{6.3}$$

where, as in figure 6, A and B lie immediately on either side of the shock. Suppose that conditions upstream of the shock (i.e. $h_A^{(s)}, u_A^{(n)}(s), u_A^{(s)}(s), c_x, \theta$) are given. Since s-derivatives are allowed, the first two terms on the right-hand side of (6.3) can be evaluated directly using (5.4) and (5.5). It remains to find an expression for $\partial u^{(s)}/\partial n$ in terms of s-derivatives alone. The tangential component of (6.1) with some rearrangement is

$$\frac{\partial u^{(s)}/\partial n}{h} = \frac{1}{h(c-u^{(n)})}\left(c_x \sin\theta \frac{\partial u^{(s)}}{\partial s} + u^{(s)}\frac{\partial u^{(s)}}{\partial s} + u^{(n)} + \frac{\partial h}{\partial s} + \frac{\partial b}{\partial s}\right),$$

where $c = c_x \cos\theta$ is the velocity of the shock normal to itself. The term $h(c-u^{(n)})$ is conserved in view of (5.4). Taking jumps and using (5.7) to eliminate the first two terms on the right-hand side, we find

$$\left[\frac{\partial u^{(s)}/\partial n}{h}\right]_{A}^{B} = \frac{1}{h(c-u^{(n)})}\left(\underset{A}{[}u^{(n)}\underset{B}{]} + \frac{\partial}{\partial s}\underset{A}{[}h\underset{B}{]}\right).$$

It follows from (6.3) that

$$\begin{aligned}\underset{A}{[}\phi\underset{B}{]} &= \left[\frac{1+\dfrac{\partial u^{(s)}}{\partial n} - \dfrac{\partial u^{(n)}}{\partial s}}{h}\right]_{A}^{B} = \left[\frac{u^n + \dfrac{\partial h}{\partial s}}{h(c-u^{(n)})}\right]_{A}^{B} + \left[\frac{1-\dfrac{\partial u^{(n)}}{\partial s}}{h}\right]_{A}^{B} \\ &\quad - \left[\frac{(u^{(n)}-c)\dfrac{\partial u^{(n)}}{\partial s} + \dfrac{\partial h}{\partial s}}{h(u^{(n)}-c)}\right]_{A}^{B}.\end{aligned} \tag{6.4}$$

Equation (6.4) can be further simplified if the shock forms a straight line (c = constant):

$$\begin{aligned}\underset{A}{[}\phi\underset{B}{]} &= \frac{-\left[(u^{(n)}-c)\dfrac{\partial}{\partial s}(u^{(n)}-c) + \dfrac{\partial h}{\partial s}\right]}{h(u^{(n)}-c)} \\ &= \frac{-\dfrac{\partial}{\partial s}\underset{A}{[}B\underset{B}{]}}{Vh},\end{aligned} \tag{6.5}$$

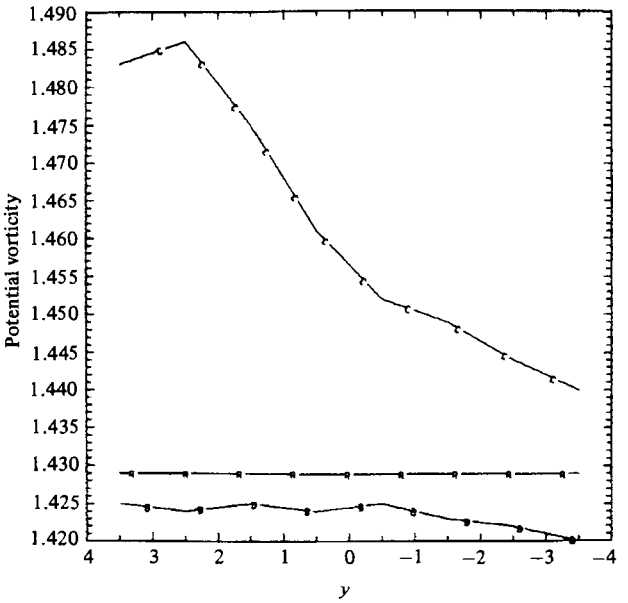

FIGURE 7. Potential vorticity profiles taken from the flow of figure 4. Section A is taken ahead of the upstream-moving bore, section B between this bore and the jump, and section C slightly downstream of the jump. The values were taken at 300 time steps, at which time the bores and jumps had become fully developed and the flow had achieved its asymptotic character.

where $V = u^{(n)} - c$ is the normal fluid velocity seen in a frame moving with the shock and $B = \frac{1}{2}(V^2 + u^{(s)2}) + h$ is the Bernoulli function based on this velocity. Vh is a conserved quantity.

Thus the change in potential vorticity is related to the rate of energy dissipation within the shock. It is possible to express $[B]_{A\ B}$ in terms of the jump in height alone (Rayleigh 1914) as

$$[\phi]_{A\ B} = \frac{1}{4Vh}\frac{\partial}{\partial s}\frac{[h]^3_{A\ B}}{h_B h_A}. \tag{6.6}$$

It is interesting to observe the values of $[\phi]_{A\ B}$ in the numerical solutions of figure 4. This information is displayed in figure 7, which contains potential-vorticity profiles at three sections along the channel. The first (labelled 'A') is taken upstream of the bore. Here ϕ = constant, as this was imposed as the initial condition. The second section (labelled 'B') was taken between the bore and the jump. Here ϕ decreases by a small amount which is probably within the limits of numerical error. The final section (labelled 'C') is taken downstream of the jump, and the potential vorticity here increases by a more significant amount.

Are these results consistent with (6.6)? First consider the hydraulic jump, for which $Vh = uh$. This jump is essentially a breaking Kelvin wave which is frozen in the supercritical flow downstream of the sill. The largest values of $[h]_{A\ B}$ thus tend to occur on the left side of the channel, that is

$$\frac{\partial}{\partial s}\left(\frac{[h]^3_{A\ B}}{h_B h_A}\right) > 0.$$

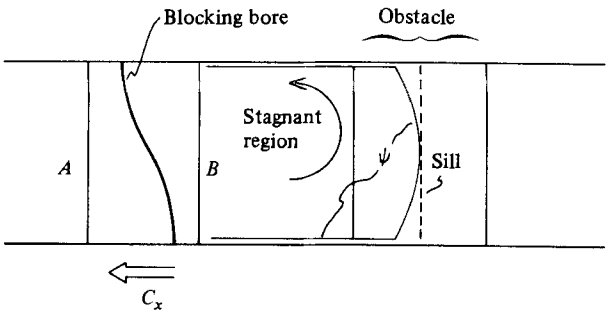

FIGURE 8. Plan view of channel showing bore moving away from obstacle and leaving behind a blocked region with cyclonic eddy.

The change in potential vorticity is therefore positive, as verified by the numerical results. This change is most intense on the near side of the channel where the boundary-layer contribution to $[h]^3_{A\ B}$ is greatest.

Analysis of the bore is also possible since the angle θ was observed to remain approximately zero throughout the upstream propagation. Equation (6.6) is then allowed with $V = u_A - c = u_A - c_x$. Since $c < 0$, the term Vh will be larger in general than the corresponding value for the jump. Furthermore the neighbouring depths h_B and h_A are somewhat larger and the change in depth $[h]_{A\ B}$ somewhat smaller. Therefore, the magnitude of $[\phi]_{A\ B}$ is less and this is again verified in figure 7.

A more precise verification of the magnitude of $[\phi]_{A\ B}$ is difficult owing to the difficulty in measuring $[h]_{A\ B}$ from numerical data. (The numerical model smears the shocks over 5 or 6 grid points and it is difficult to judge which portion of the surface breaks and which simply has a steep slope.) However, using the largest possible values of $[h]_{A\ B}$ taken from the jump at $x = 100$ in figure 4 we estimate $[\phi]_{A\ B} = 0.03$, which agrees with the order of magnitude of change indicated in figure 7.

The changes in ϕ plotted in figure 7 are small compared with ϕ itself. Hence the connection formulas (5.9)–(5.11) can be applied accurately in conjunction with (5.12) by assuming that $[\phi]_{A\ B} = 0$. It would be possible to construct the solution for large time to the initial-value problem by connecting the asymptotic flow to the initial flow using the jump conditions (5.9) and (5.10), and the conservation of the appropriate Riemann function across the rarefaction wave. This computation is not carried out here, but Houghton & Kasahara (1968) used the procedure successfully in connection with the non-rotating analogue of the problem.

7. Total blockage by the obstacle

We expect that a semigeostrophic channel flow will be completely blocked if the obstructing obstacle is high enough or if a sufficient decrease in the upstream energy of the flow occurs (as often takes place in the deep ocean). Although this situation is difficult to model numerically, we can piece together a scenario describing the blockage and predict the required obstacle height by extrapolating the numerical

results for partial blockage. The following discussion assumes the initial potential vorticity to be uniform and the change in potential vorticity across the blocking bore to be $O(\delta)$, as occurs in the numerical results. Although there is no guarantee that $[\phi]_{A}^{B}$ will continue to be small for large bores, it is hoped that the following analysis will provide a starting point and spur experimental investigation into the problem. We will limit the discussion to initially subcritical flows.

As before, we assume that the blockage will be accomplished through formation of a bore which moves upstream from the obstacle, leaving behind a blocked region (figure 8). If the flow in the blocked region (labelled B) is steady, then

$$Q = \int_{-w}^{+w} u_B h_B \,\mathrm{d}y = \tfrac{1}{2}(h_{B+}^2 - h_{B-}^2) = 0,$$

in view of (2.5).

The depth on either wall is therefore the same:

$$h_{B+} = h_{B-}. \tag{7.1}$$

Since no fluid passes the sill, the streamline at $+w$ connects with that at $-w$. Therefore the Bernoulli law demands that

$$u_{B+}^2 = u_{B-}^2 \tag{7.2}$$

away from the obstacle. Furthermore, since $u = 0$ at the sill, the obstacle must have height

$$b_{\mathrm{b}} = \tfrac{1}{2}u_{B+}^2 + h_{B+} = \tfrac{1}{2}u_{B-}^2 + h_{B-}. \tag{7.3}$$

If the change in potential vorticity across the bore is $O(\delta)$ then (3.1)–(3.8) continue to hold in the blocked region. In this case (3.7) gives

$$\bar{u} = -\phi^{\frac{1}{2}}T^{-1}\Delta h = 0,$$

so that the negative root of (7.2) is appropriate:

$$u_{B-} = -u_{B+}. \tag{7.4}$$

Using (7.1) and (7.4) with (3.1)–(3.6) it follows that

$$\left.\begin{aligned} h_B(x,y) &= \phi^{-1} + (h_+(x) - \phi^{-1})\frac{\cosh(\phi^{\frac{1}{2}}y)}{\cosh(\phi^{\frac{1}{2}}w)}, \\ u_B(x,y) &= \phi^{\frac{1}{2}}(\phi^{-1} - h_+(x))\frac{\sinh(\phi^{\frac{1}{2}}y)}{\cosh(\phi^{\frac{1}{2}}w)}. \end{aligned}\right\} \tag{7.5}$$

The circulation in the blocked region therefore consists of a cyclonic eddy that is symmetric with respect to y (figure 8). Away from the obstacle the flow is uniform with respect to x, implying that $v = 0$. The recirculation is fed over the topography, where approaching fluid is turned to the left and develops an $O(\delta)$ cross-channel velocity.

Under these assumptions, it is possible to predict the blocking height b_{b}, given the initial flow rate Q_0 and energy B_0. Applying (5.10) across the bore gives

$$c_x \int_{-w}^{w} (h_B - h_A)\,\mathrm{d}y = -\int_{-w}^{w} u_A h_A \,\mathrm{d}y = -Q_0.$$

Using (3.3) to evaluate the left-hand integral, we find

$$c_x = \frac{Q\phi^{\frac{1}{2}}}{2T}(\bar{h}_A - h_{B+})^{-1}.$$

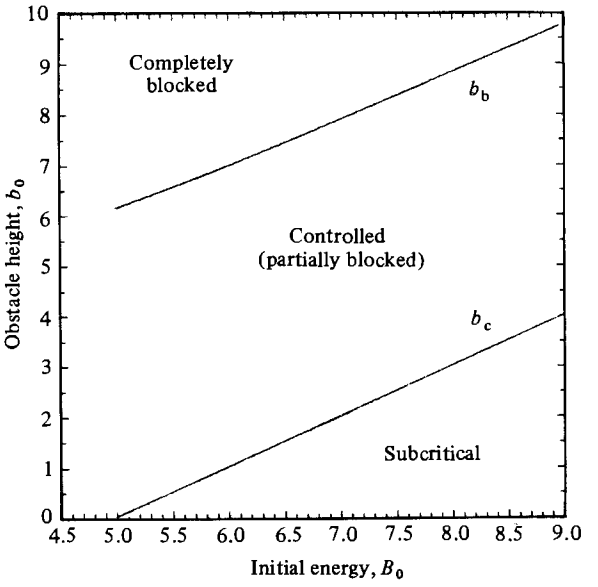

FIGURE 9. Asymptotic states for initially subcritical flow with $Q_0 = \phi_0 = 1$. Uniform initial states for $B_0 < 5.0$ do not exist.

Application of (5.11) on either wall and summation of the results also gives

$$-c_x(u_{A+}h_{A+}+u_{A-}h_{A-}) = 2u_{B+}^2 h_{B+}+h_{B+}^2-(u_{A+}^2 h_{A+}+\tfrac{1}{2}h_{A+}^2+u_{A-}^2 h_{A-}+\tfrac{1}{2}h_{A-}^2).$$

Elimination of c_x between the above two equations and use of (7.5) results in a single equation for h_{B+} in terms of the initial state:

$$h_{B+}^4+[\phi^{-1}(\tfrac{1}{2}T^{-2}-2)-\bar{h}_A]h_{B+}^3+[\phi^{-2}-\phi^{-1}(\tfrac{1}{2}T^{-2}-2)\bar{h}_A]h_{B+}^2$$
$$-[\tfrac{1}{2}\phi^{-1}T^{-2}Q_2+\bar{h}_A]h_{B+}+\tfrac{1}{2}\phi^{-1}T^{-2}Q_2\bar{h}_A-\tfrac{1}{2}T^{-1}Q_0Q_1\phi^{\frac{1}{2}}=0, \quad (7.6)$$

where

$$Q_1 = u_{A+}h_{A+}+u_{A-}h_{A-},$$
$$Q_2 = u_{A+}^2 h_{A+}+\tfrac{1}{2}h_{A+}^2+u_{A-}^2 h_{A-}+\tfrac{1}{2}h_{A-}^2.$$

Once h_{B+} is found from (7.6) then b_b is computed from (7.3) and (7.5) as

$$b_b = \tfrac{1}{2}u_{B+}^2+h_{B+} = \tfrac{1}{2}\phi T^2(\phi^{-1}-h_{B+})^2+h_{B+}.$$

Once again, it is worthwhile mentioning the conditions under which this theory is valid. First, the blocked region must be in a steady state and no streamline must cross the sill. Secondly, the bore and its bordering dispersive boundary must have settled into an equilibrium state characterized by a single velocity c_x. Finally, the change in potential vorticity from its initial unform value must be $\leqslant O(\delta)$ across the blocking bore, as in the solutions of figure 4.

Figure 9 shows the behaviour of b_b as a function of the initial energy B_0. Also shown is a plot of the corresponding values of critical obstacle height b_c as computed from (4.2) and (4.3).

8. Discussion

For two distributions (uniform and linear) of initial potential vorticity, it has been shown that the initial stages of semigeostrophic adjustment proceeds in a similar way

to the non-rotating adjustment observed by Long (1954, 1970) and Houghton & Kasahara (1968). The Kelvin waves that occur in the present problem play the same roles that long gravity waves do in the earlier work. However, the breakage of the Kelvin waves and consequent shock formation introduces complications not present in the earlier work. Specifically, the calculation of the asymptotic state (as $t \to \infty$) through construction of a weak semigeostrophic solution depends upon knowing the jumps in potential vorticity across the shocks. Although a jump in potential vorticity can be related to the physical process of dissipation through (6.6) it is difficult to use this information to construct a connection formula. This difficulty is primarily due to the complexity of the dispersive regions connecting the shock to the neighbouring semigeostrophic flows. Bulk connection formulas, such as (5.9), require an assumption concerning the jump in potential vorticity in order to be valid.

The overwhelming majority of the work to date in the area of rotating hydraulics has been devoted to steady flows of uniform potential vorticity. We have endeavoured to show, however, that physical processes which lead to the establishment of a hydraulically controlled state may render the potential vorticity non-uniform, even when the adjustment occurs from an initial state of uniform potential vorticity. This does not diminish from the value of the earlier work; indeed the numerical results indicate that the non-uniformity induced during the adjustment can be small. The present need, however, is for a greater understanding of the behaviour of flows containing non-uniform potential vorticity. The results of the numerical computations of §4 suggest that the adjustment of semigeostrophic flows of non-uniform ϕ is similar to that of uniform-ϕ flows, at least over the short timescales observed. It is not clear, however, what additional adjustment or instability might occur on longer timescales.

There is also a need for further study of rotating shocks and their connection properties particularly with regard to the way in which potential vorticity is altered. For example, what is the structure of a shock propagating in a region of flow separation? Also, can shocks of larger amplitude than those produced in §4 significantly alter the potential vorticity of passing fluid? If so, the change may have implications for the stability of the downstream flow. Semigeostrophic instability is a problem which has only begun to be explored (see Orlanski 1968; Griffiths, Killworth & Stern 1982). In the ocean, however, we envision the flow downstream of the obstacle emptying into a large basin and the dynamics becoming quasigeostrophic there. The barotropic stability of the flow will then depend on the Fjortoft (1952) criterion that $\mathrm{d}\phi/\mathrm{d}\psi$ must vanish for instability to occur. However, in the absence of friction the potential-vorticity gradient $\mathrm{d}\phi/\mathrm{d}\psi$ can be traced back to the overflow which may contain a hydraulic jump. The structure of the jump may then control the stability of the downstream flow since $\phi(\psi)$ is set at the jump. It is the author's opinion that such questions may be difficult to resolve numerically and that laboratory experiments may be more suitable.

This work was supported by the National Science Foundation under Grant OCE 78-25405. The numerical computations were carried out at the National Center for Atmospheric Research under project 35781011. The author wishes to thank N. Hogg, J. Pedlosky, J. Whitehead, M. Hall, G. Flierl and E. Mollo-Christensen for many useful discussions concerning the problem, and M. Lucas for help in preparation of the manuscript.

Appendix A. Numerical method

The numerical method is based on a finite-difference scheme introduced by Lax & Wendroff (1960) and discussed in the textbook of Roache (1972). The scheme is designed to simulate systems of equations containing one spatial dimension written in conservation-law form. The conserved quantities (in the present case mass and momentum flux) implied by the conservation laws will also tend to be conserved in the numerical scheme, even in the presence of shocks. Because of this feature, the Lax–Wendroff method has been used successfully by a number of authors to compute solutions containing shocks.

It is possible to extend the original Lax–Wendroff method to two spatial dimensions; however the numerical scheme is extremely cumbersome and time-consuming (Roache 1972). A more economical version is a two-step variation of the Lax–Wendroff method introduced by Richtmeyer (1963), which requires an intermediate calculation to be done between each time step. Although less is known about the properties of the two-step difference equations, the method has been tested successfully in connection with shallow-water wave problems (Sielecki & Wurtele 1970) and aerodynamic shock computations (Rubin & Burstein 1967). The difference equations used correspond to those listed by Sielecki and Wurtele.

Unfortunately, the stability properties of two-dimensional two-step Lax–Wendroff methods are worse than those of the one-dimensional method (Roache 1972). For example, the numerical oscillations that occurred downstream of the free-surface shocks in the adjustment experiments of §3 (see figures 4 and 5) initially proved to be unacceptably large. For this reason an artificial damping term of the form

$$\nu \frac{\partial}{\partial x}\left(h \frac{\partial u}{\partial x}\left|\frac{\partial u}{\partial x}\right|\right) \tag{A 1}$$

was added to the x-momentum balance in order to damp disturbances with short wavelengths. The constant ν is a pseudoviscosity, which typically had a value between 0.5 and 1.

A 15×400 grid was used to form the channel, with the obstacle centred between rows 250 and 300. The sidewall boundary conditions were imposed by setting $v = 0$ at sidewall grid points and extrapolating from the interior values of u and h through a second-order Taylor expansion. The difference calculation was carried out until the transients resulting from the adjustment near the obstacle collided with the ends of the grid or until the numerical oscillations grew unacceptable.

Appendix B. Derivation of (5.9)

Referring to figure 6, we consider a shock whose position $x = \eta(y,t)$ changes according to $\eta_t = c_x = \text{constant}$. The line $x = A(y,t)$ and $x = B(y,t)$ lie slightly upstream and downstream of η, and $x = A'(t)$ and $x = B'(t)$ represent the upstream and downstream extents of the dispersive region bordering the shock.

First consider the momentum flux at the bore itself. From (5.5) and (5.6) we can write

$$\underset{A}{[}(c-u^{(n)})\,u^{(n)}h - \tfrac{1}{2}h^2\underset{B}{]}\cos\theta + \underset{A}{[}(c-u^{(n)})\,u^{(s)}h\underset{B}{]}\sin\theta = 0,$$

as both bracketed terms are identically zero. The normal speed c is related to the x-speed though $c = c_x \cos\theta$. From this it follows that

$$\underset{A}{[}(c-u^{(n)})\,uh - \tfrac{1}{2}h^2\cos\theta\underset{B}{]} = 0. \tag{B 1}$$

For translating disturbances with permanent form and speed c_x the x-momentum flux (5.1) can be written as

$$\nabla\cdot\{(u-c_x)\,uh+\tfrac{1}{2}h^2,\,uvh\}=-h\left(\frac{\mathrm{d}b}{\mathrm{d}x}-v\right).$$

Integrating over the upstream dispersive region (labelled R_A in figure 6) and applying the divergence theorem gives

$$\int_{\partial R_A}\{(u-c_x)\,uh+\tfrac{1}{2}h^2,\,uvh\}\cdot\mathrm{d}\hat{\boldsymbol{n}}=-\int_{R_A}h\left(\frac{\mathrm{d}b}{\mathrm{d}x}-v\right)\mathrm{d}\sigma,$$

where $\hat{\boldsymbol{n}}$ is the unit normal to ∂R_A. Along each wall, where $\hat{\boldsymbol{n}}=(0,1)$ and $v=0$, the contour integral vanishes. Along the upstream border of R_A, where $x=A'$, we have $\hat{\boldsymbol{n}}=(1,0)$. Therefore

$$\begin{aligned}&\int_{\partial R_A}\{(u-c_x)\,uh+\tfrac{1}{2}h^2,\,uvh\}\cdot\mathrm{d}\hat{\boldsymbol{n}}\\&=\int_{-w}^{w}\{(u-c_x)\,uh+\tfrac{1}{2}h^2\}_{A'}\,\mathrm{d}y-\int_{s(-w)}^{s(w)}\{(u^{(n)}-c)\,uh+\tfrac{1}{2}h^2\}_A\,\mathrm{d}s\\&=-\iint_{R_A}h\left(\frac{\mathrm{d}b}{\mathrm{d}x}-v\right)\mathrm{d}\sigma,\end{aligned}\tag{B 2}$$

with s measured along the bore.

Following the same procedure in R_B, subtracting the result from (B 2), and applying (B 1) finally gives

$$\left[\int_{-w}^{w}\{(u-c_x)\,uh+\tfrac{1}{2}h^2\}\,\mathrm{d}y\right]_{A'}^{B'}=-\iint_{R_A+R_B}h\left(\frac{\mathrm{d}b}{\mathrm{d}x}-v\right)\mathrm{d}\sigma.$$

REFERENCES

Baines, P. O. & Davies, P. A. 1980 Laboratory studies of topographic effects in rotating and/or stratified fluids. In *Orographic Effects in Planetary Flows, GARP Publ. Ser.* no. 23. World Met. Orgn.

Blumen, W. 1972 Geostrophic adjustment. *Rev. Geophys.* **10**, 485–528.

DaFermos, C. M. 1974 Quasilinear hyperbolic systems that result from conservation laws. In *Nonlinear Waves* (ed. S. Leibovich & A. R. Seebass), pp. 82–100. Cornell University Press.

Fjortoft, R. 1951 Stability properties of large scale atmospheric disturbances. In *Meteorology*, pp. 454–000. *Am. Met. Soc.*

Gill, A. E. 1976 Adjustment under gravity in a rotating channel. *J. Fluid Mech.* **77**, 603–621.

Gill, A. E. 1977 The hydraulics of rotating-channel flow. *J. Fluid Mech.* **80**, 641–671.

Gill, A. E. & Schumann, E. H. 1979 Topographically induced changes in the structure of a coastal inertial jet: applications to the Agulhas Current. *J. Phys. Oceanogr.* **9**, 975–991.

Griffiths, R. W., Killworth, P. D. & Stern, M. E. 1982 Ageostrophic instability of ocean currents. *J. Fluid Mech.* **117**, 343–377.

Houghton, D. D. & Kasahara, A. 1968 Nonlinear shallow fluid flow over an isolated ridge. *Communs Pure Appl. Maths* **21**, 1–23.

Klemp, J. B. & Lilly, D. K. 1975 The dynamics of wave-induced downslope winds. *J. Atmos. Sci.* **32**, 320–339.

Lax, P. & Wendroff, B. 1960 Systems of conservation laws. *Communs Pure Appl. Maths* **13**, 217–237.

LONG, R. R. 1954 Some aspects of the flow of stratified fluids II. Experiments with a two-fluid system. *Tellus* **5**, 42–58.

LONG, R. R. 1970 Blocking effects in flow over obstacles. *Tellus* **22**, 471–480.

ORLANSKI, I. 1968 Instability of frontal waves. *J. Atmos. Sci.* **25**, 178–200.

PEDLOSKY, J. 1979 *Geophysical Fluid Dynamics*. Springer.

RAYLEIGH, LORD 1914 On the theory of long waves and bores. *Proc. R. Soc. Lond.* **A90**, 324–328.

RICHTMYER, R. D. 1963 A survey of difference methods for nonsteady fluid dynamics. *NCAR Tech. Note* 63–2, *Boulder, Colorado.*

ROACHE, P. J. 1972 *Computational Fluid Dynamics*. Hermosa.

RUBIN, E. L. & BURSTEIN, S. Z. 1967 Difference methods for the invisicid and viscous equations of a compressible gas. *J. Comp. Phys.* **2**, 178–196.

SHEN, C. Y. 1981 The rotating hydraulics of open-channel flow between two basins. *J. Fluid Mech.* **112**, 161–188.

SIELECKI, A. & WURTELE, M. G. 1970 The numerical integration of the nonlinear shallow-water equations with sloping boundaries. *J. Comp. Phys.* **6**, 219–236.

STERN, M. E. 1974 Comment on rotating hydraulics. *Geophys. Fluid Dyn.* **6**, 127–130.

STOKER, J. J. 1957 *Water Waves*. Interscience.

WHITEHEAD, J. A., LEETMAA, A. & KNOX, R. A. 1974 Rotating hydraulics of strait and sill flows. *Geophys. Fluid Dyn.* **6**, 101–125.

WHITHAM, G. B. 1974 *Linear and Nonlinear Waves*. Wiley.

WORTHINGTON, L. V. 1969 An attempt to measure the volume transport of Norwegian Sea overflow water through the Denmark Strait. *Deep-Sea Res.* **16** (*Suppl.*), 421–433.